Proceedings of the ASME 2021
International Design Engineering Technical Conferences and
Computers and Information in Engineering Conference
IDETC-CIE2021
August 17-19, 2021, Virtual, Online

DETC2021-67884

DESIGN OF FOUR-PATCH MULTI-STABLE COMPOSITE LAMINATES FOR SHAPE MORPHING APPLICATIONS

Jebin Biju¹, Georges Fadel¹, Suyi Li¹, Oliver Myers¹

¹Department of Mechanical Engineering, Clemson University, Clemson, USA

ABSTRACT

Thin bistable composite laminates can be used for shape morphing applications by virtue of their material properties and asymmetric ply layup. These laminates are called bistable because they can be snapped into two or more stable shapes. A single bistable patch can result in simple cylindrical shapes and when multiple such patches are assembled into a single multipatch laminate they result in more complex shapes and multiple stable shapes that can find wide practical use in shape morphing applications. Analytical models exist that can approximate the stable shapes of the laminates from the input of material properties and laminate geometry. And these models correlate with FEA and experiment to a satisfactory degree and could be used for the design of multi patch laminates. In this research, we make use of these analytical models that solve for a four-patch grid laminate and create a design method based on optimization to solve the reverse problem to arrive at the laminate parameters given the target shape(s). Two approaches are presented wherein one targets a single stable shape and the other targets two stable shapes which are the shapes before and after snap through. This work would be useful to understand how multi-patch laminates could be designed using optimization.

Keywords: Smart Materials and Structures, Multiobjective Optimization, Design Optimization

1. INTRODUCTION

When cured flat in a press or autoclave, thin composite laminates with an asymmetric fiber layout develop a curvature upon cooling back to room temperature. This occurs due to the thermal expansion mismatch between the plies of different fiber orientation. The induced residual thermal stresses in the laminates makes them warp and develop the aforementioned curvature which is cylindrical for a single patch laminate [1,2]. It is also observed that these laminates have another cylindrical configuration post curing which can be obtained by applying an

external force or excitation at some locations on the patch. This process is called snap through of the laminate. The configurations are referred to as states, and are called presnapped or post-snapped states [3]. The shape of the asymmetric patch can be altered by imposing boundary conditions on the edges of that patch. In this context, a patch is referred to as the section of the laminate which has the same fiber orientation for the individual plies. Patches may have different shapes, dimensions, number of plies, ply thicknesses, etc., but may have the same ply layup. The implementation potential of single patch bistable composite laminates would be severely constrained since their external shapes in stable equilibria resemble only cylindrical surfaces. The lack of sophisticated shape changes between stable states prevents developing other promising adaptive functions that exploit this function. Thus, expanding on the bi-stability idea, and since boundary conditions can alter the shape of a patch, we should be able to assemble multiple asymmetric and/or symmetric laminates to have a multi-patch laminate as shown in Figure 1, which could have 2^n shapes, where n is the number of bistable patches in the laminate. Thus, making these laminates multi-stable.

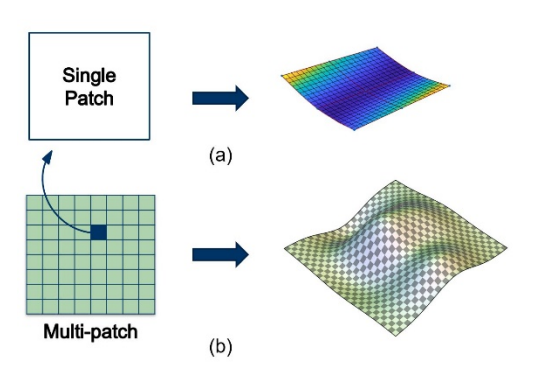


FIGURE 1: (a) SINGLE PATCH (b) MULTI-PATCH LAMINATE

These laminates would be much more suitable for practical shape morphing applications since multiple connected patches which are individually bistable would result in a shape significantly more complex than the cylindrical shape. A popular application in the literature for such morphing potential is its use in aerospace structures, where the bistable laminates are used as the trailing edge or an internal structure to allow shape morphing of the wing [4,5].

In their work, Hyer and Dano [1] presented an analytical model using the Rayleigh Ritz technique to compute the shape of a single bistable patch with cross-ply layup, where the top and bottom plies had a difference of 90° ; and made comparisons with FEA and experimental data. The analytical model captured the shape for the most part, except for slight deviations at the edges. Schlecht and Schulte[2] performed an FEA study for single patch $[0_2/90_2]$ laminates comparing them with the results from Hyer's analytical model and observed "edge effects" which made the laminate take up a slight saddle shape at the edges. These deviations were also observed in the experimental study by Betts et al[6] when correlated with analytical results.

However, the consensus in the literature is that the analytical approach works reasonably well in predicting the shapes of asymmetric composite laminates. Since we need an approximate representation to be able to design the desired shapes, we can use these models as a tool to design multi-patch laminates; but we need to do so with caution and use the model in conjunction with FEA to converge and ultimately confirm a match with the targeted shape.

2. ANALYTICAL MODEL

As discussed earlier, Hyer's model predicts the shapes of single patch laminates. A recent addition to the literature is the model by Algmuni et. al.[7] for a four-patch grid laminate. It is an extension of Hyer's model[1] but with added continuity constraints at the common edges of the patches, like those by Mattioni[8] to tie the four patches. From the above literature, the equations to setup the model for an n^{th} patch in an n patch laminate can be given as follows. All the following quantities and approximations are made for the n^{th} patch.

The strain energy for the n^{th} patch is given by,

$$\Pi^{(n)} = \int_{-D_{y}^{(n)}/2}^{D_{y}^{(n)}/2} \int_{2}^{D_{x}^{(n)}/2} \frac{1}{2} \begin{bmatrix} \varepsilon^{0} \\ \kappa^{0} \end{bmatrix} \begin{bmatrix} A_{ij} & B_{ij} \\ B_{ij} & D_{ij} \end{bmatrix} \begin{bmatrix} \varepsilon^{0} \\ \kappa^{0} \end{bmatrix} - \begin{bmatrix} N \\ M \end{bmatrix} \begin{bmatrix} \varepsilon^{0} \\ \kappa^{0} \end{bmatrix} dx dy$$
(1)

Where, $\Pi^{(n)}$ is the strain energy, $D_x^{(n)}$ and $D_y^{(n)}$ are the x, y dimensions of the n^{th} patch, ε^0 is the mid-plane strain, and κ^0 is the curvature of the laminate.

 A_{ij} , B_{ij} , D_{ij} are the extensional, bending-extension and bending stiffnesses, respectively. For the k^{th} layer in a P-ply laminate where the z-height of the k^{th} layer is denoted by z_k ; the stiffnesses are given by Eq(2). In this study we deal with a four-patch laminate with two plies, hence n=4 and P=2.

$$A_{ij} = \sum_{k=1}^{P} (\bar{Q}_{ij})_{k} (z_{k} - z_{k-1})$$

$$B_{ij} = \frac{1}{2} \sum_{k=1}^{P} (\bar{Q}_{ij})_{k} (z_{k}^{2} - z_{k-1}^{2})$$

$$D_{ij} = \frac{1}{3} \sum_{k=1}^{P} (\bar{Q}_{ij})_{k} (z_{k}^{3} - z_{k-1}^{3})$$
(2)

N, M are the resultant force and moment matrices which are given by,

$$[N] = \Delta T \sum_{k=1}^{P} \begin{bmatrix} \overline{Q}_{11} & \overline{Q}_{12} & \overline{Q}_{16} \\ \overline{Q}_{21} & \overline{Q}_{22} & \overline{Q}_{26} \\ \overline{Q}_{16} & \overline{Q}_{26} & \overline{Q}_{66} \end{bmatrix} \times \begin{bmatrix} \alpha_{x} \\ \alpha_{y} \\ \alpha_{xy} \end{bmatrix}_{k} (z_{k} - z_{k-1})$$

$$[M] = \frac{1}{2} \Delta T \sum_{k=1}^{P} \begin{bmatrix} \overline{Q}_{11} & \overline{Q}_{12} & \overline{Q}_{16} \\ \overline{Q}_{21} & \overline{Q}_{22} & \overline{Q}_{26} \\ \overline{Q}_{16} & \overline{Q}_{26} & \overline{Q}_{66} \end{bmatrix} \times \begin{bmatrix} \alpha_{x} \\ \alpha_{y} \\ \alpha_{xy} \end{bmatrix}_{k} (z_{k}^{2} - z_{k-1}^{2})$$

$$(3)$$

Here, $(\bar{Q}_{ij})_k$ is the reduced transformed stiffness matrix, α_x , α_y , α_{xy} are the transformed thermal expansion coefficients and ΔT is the temperature change during curing.

Approximations for the out-of-plane displacement w^0 and midplane strains ε_x^0 , ε_y^0 are given by,

$$\begin{split} w^{0(n)} &= w_{22}{}^{(n)}x^2y^2 + w_{21}{}^{(n)}x^2y + w_{12}{}^{(n)}xy^2 + w_{20}{}^{(n)}x^2 \\ &+ w_{02}{}^{(n)}y^2 + w_{11}{}^{(n)}xy + w_{10}{}^{(n)}x + w_{01}{}^{(n)}y + w_{00}{}^{(n)} \\ \varepsilon_x^{0(n)} &= \varepsilon_{x00}{}^{(n)} + \varepsilon_{x11}{}^{(n)}xy + \varepsilon_{x20}{}^{(n)}x^2 + \varepsilon_{x02}{}^{(n)}y^2 \\ \varepsilon_y^{0(n)} &= \varepsilon_{y00}{}^{(n)} + \varepsilon_{y11}{}^{(n)}xy + \varepsilon_{y20}{}^{(n)}x^2 + \varepsilon_{y02}{}^{(n)}y^2 \end{split}$$

$$(4)$$

The in-plane displacements can now be calculated and are given by,

$$u^{0(n)} = \int \left(\varepsilon_x^{0(n)} - \frac{1}{2} \left(\frac{\partial w^{0(n)}}{\partial x}\right)^2\right) dx + h^{(n)}(y)$$

$$v^{0(n)} = \int \left(\varepsilon_y^{0(n)} - \frac{1}{2} \left(\frac{\partial w^{0(n)}}{\partial y}\right)^2\right) dy + g^{(n)}(x)$$
(5)

Where, $h^{(n)}(y)$ and $g^{(n)}(x)$ are added because of partial integration to suppress rigid body rotation

$$h^{(n)}(y) = u_{01}^{(n)}y + u_{03}^{(n)}y^3$$

$$g^{(n)}(x) = v_{10}^{(n)}x + v_{30}^{(n)}x^3$$
(6)

The shear strain can now be defined by,

$$\varepsilon^0 = \begin{bmatrix} \varepsilon_x^0 & \varepsilon_y^0 & \gamma_{xy}^0 \end{bmatrix}^T \tag{7}$$

The curvatures in the x, y and twist directions are given by,

$$\kappa^{0} = \begin{bmatrix} -\frac{\partial^{2} w^{0}}{\partial x^{2}} \\ -\frac{\partial^{2} w^{0}}{\partial y^{2}} \\ -2\frac{\partial^{2} w^{0}}{\partial x \partial y} \end{bmatrix}$$
(8)

In summary the design variables for this level are the unknown coefficients used for the approximations in equations (4) & (6). The set of unknown coefficients for a particular patch are denoted by c_n where, as mentioned earlier, n is the patch number in the laminate.

$$c_{n} = [w_{22}, w_{21}, w_{12}, w_{20}, w_{02}, w_{11}, w_{10}, w_{01}, w_{00}, \varepsilon_{x00}, \varepsilon_{x02}, \varepsilon_{x11}, \varepsilon_{x20}, \varepsilon_{y00}, \varepsilon_{y11}, \varepsilon_{y20}, \varepsilon_{y02}, u_{01}, u_{03}, v_{10}, v_{30}]^{(n)}$$

$$(9)$$

Thus, for a four-patch laminate the sets of unknown coefficients would be c_1, c_2, c_3, c_4 .

Total strain energy for a laminate with n patches is given by the sum of energies of all patches.

$$\Pi_{total} = \sum_{n=1}^{P} \Pi^{(n)} \tag{10}$$

The total strain energy of the laminate is thus a function of the coefficients of each patch. From equations (1), (3) & (10) we see that the strain energy is a function of the following physical quantities (i) the reduced transformed stiffness matrix and thus a function of the fiber orientations (ii) ply thickness, (iii) patch dimensions, and finally (iv) material properties of the composite laminate. Thus, the strain energy could be minimized to solve for the coefficients of the approximations (c_n) and thereby predict the shape of the laminate.

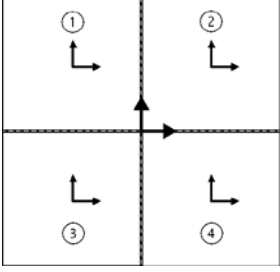


FIGURE 2: 4-PATCH GRID GEOMETRY AND COORDINATE SYSTEM

Since we are solving for a multi-patch laminate, we need to enforce continuity constraints between the patch edges to ensure that all the patches are connected. From the work by Algmuni et al., we know that the continuity constraints for a four-patch grid laminate (n = 4) as represented in Figure 2, can be defined as shown in the Table 1 below.

TABLE 1: CONTINUITY CONSTRAINTS AT COMMON EDGES FOR FOUR-PATCH GRID LAMINATE[7]

Along y-axis $(n = 1, 3)$	Along x-axis $(n = 1, 2)$
$u^{(n)}(0,y) = u^{(n+1)}(0,y)$	$u^{(n)}(x,0) = u^{(n+2)}(x,0)$
$v^{(n)}(0,y) = v^{(n+1)}(0,y)$	$v^{(n)}(x,0) = v^{(n+2)}(x,0)$
$w^{(n)}(0,y) = w^{(n+1)}(0,y)$	$w^{(n)}(x,0) = w^{(n+2)}(x,0)$
$\frac{\partial w^{(n)}}{\partial x}(0,y) = \frac{\partial w^{(n+1)}}{\partial x}(0,y)$	$\frac{\partial w^{(n)}}{\partial x}(x,0) = \frac{\partial w^{(n+2)}}{\partial x}(x,0)$
$\frac{\partial w^{(n)}}{\partial y}(0,y) = \frac{\partial w^{(n+1)}}{\partial y}(0,y)$	$\frac{\partial w^{(n)}}{\partial y}(x,0) = \frac{\partial w^{(n+2)}}{\partial y}(x,0)$

The above model is used to solve for the laminates in Figure 3 and 4, and their results are compared with those from FEA. All the processing in this work has been done on an Intel i7-8750H processor with 8GB RAM and 6 cores. To compare the analytical with the FEA shape, 9 fit-points are selected on the analytical result, one at each corner of the four patches, and are compared with the fit-points from the finite element result. The laminates being compared have a total size of 200*200mm and the individual patches are 100*100mm. The material properties of AS4 8552 carbon composite prepregs used in this study are listed in Table 2. Additionally, the temperature difference during cuing is set to $\Delta T = -125K$.

TABLE 2: CFRP MATERIAL PROPERTIES

Material Properties			
E_1	135e9 Pa		
E_2	9.5e9 Pa		
G_{12}	5e9 Pa		
ν_{12}	0.3		
α_{11}	-2e-8K ⁻¹		
α_{22}	3e-5K ⁻¹		
α_{33}	3e-5K ⁻¹		

As seen in Figure 3 and 4, the analytical results deviate from the finite element ones at the corner points. The deviation from the FEA results stand at a maximum of 4% relative to the side of the laminate. These deviations could be attributed to some of the assumptions made in the Classical Laminate theory which is the foundation of this approach. CLT does not take the interlaminar stresses σ_z , τ_{xz} , τ_{yz} into consideration which are responsible for causing delamination at the edges of the laminate. This causes a contradiction while balancing the stresses at the boundary [9]. Despite these issues we can make use of the analytical model to target specific shapes since it captures the overall nature of the surface relatively well. Also, the analytical model predicts the shapes of the four-patch laminates in under a minute, while FEA usually takes 7-10 minutes to simulate the curing and snap through of the laminate.

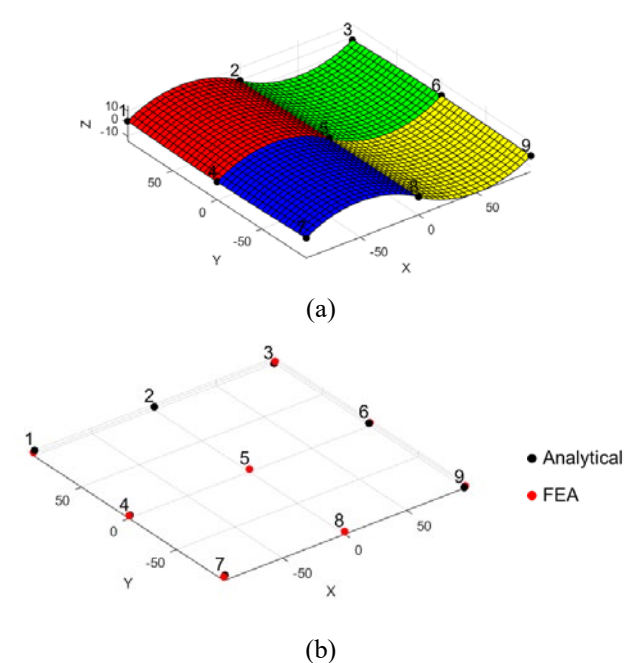


FIGURE 3: [90/0], [0/90], [90/0], [0/90] PATCH RESULTS, (a) ANALYTICAL SHAPE, (b) COMPARING ANALYTICAL WITH FEA SHAPE

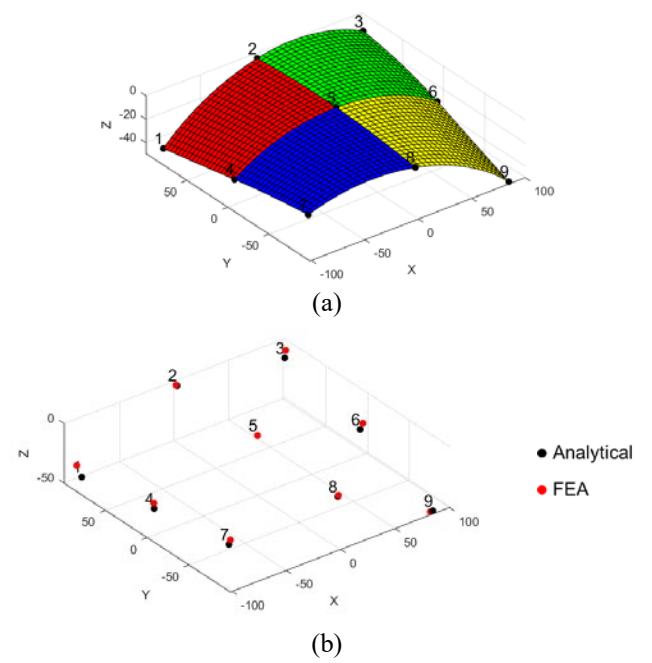


FIGURE 4: [90/0], [30/0], [50/0], [60/0] PATCH RESULTS, (a) ANALYTICAL SHAPE, (b) COMPARING ANALYTICAL WITH FEA SHAPE

3. DESIGN METHOD

As stated earlier, the goal is to optimize to a specific target shape for a surface made of multiple patches. From the discussion above we see that Algmuni's model can predict the shape of a four-patch grid laminate from the input of the laminate parameters like fiber orientation, patch dimensions, etc. We can thus set up an optimization model to solve the reverse problem and determine the laminate properties which would result in a specific target shape. The analytical model described above would be the simulation component for the optimization. The workflow should have a nested optimization setup, where the lower-level or the inner loop would predict the shape of the laminate by minimizing its total strain energy, while the higher-level optimization or the outer loop would minimize the fitness function that describes the difference between the obtained shape from lower-level (analytical shape) and the target shape (user input).

The optimization setup for both the levels is as follows:

Lower level or Inner loop:

In the case of a four-patch laminate the total strain energy would be as follows,

$$\Pi_{total} = \Pi_1 + \Pi_2 + \Pi_3 + \Pi_4 \tag{11}$$

 Π_{total} is the quantity to be minimized, while $\Pi_1, \Pi_2, \Pi_3, \Pi_4$ are the potential energies of the individual patches.

The lower-level optimization can thus be setup as follows,

minimize
$$\Pi_{total}$$
 subject to Continuity constraints D.V c_1, c_2, c_3, c_4

Higher level or Outer loop:

As stated above, the lower-level optimization solves for the unknown coefficients (c_1, c_2, c_3, c_4) and hence the shape of the four-patch laminates for a given configuration. The shape of the laminate can now be obtained from the displacement equations in equations (4) & (5). Using the shape obtained from the lower level we minimize a fitness function that compares the obtained shape with the target shape.

To simplify the problem, initially we consider a two-ply four-patch laminate where the lower ply is considered to have a fiber orientation of 0° . The orientations of the top four-patches $\theta_1, \theta_2, \theta_3 \& \theta_4$ are considered as design variables. Additionally, the laminate size is kept constant at 200*200 mm; and to parameterize the individual patch sizes, the dimensions of the top right or second patch, x' & y' are also set as variables (Figure 5). Thus, we can tap into a wider design space with the possibility of having unequal patch sizes.

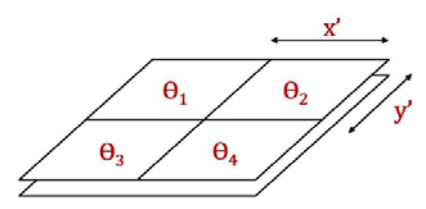


FIGURE 5: DESIGN VARIABLES FOR LOWER LEVEL

To compare the analytical and the target shapes, fit points are selected across the laminate (Figure 6). The fitness function comparing the two shapes involves calculating the deviation in coordinates of the fit points of the two surfaces. The objective function could thus be to minimize the sum of squares of the difference between the analytical and the target coordinates as shown in Eq(12).

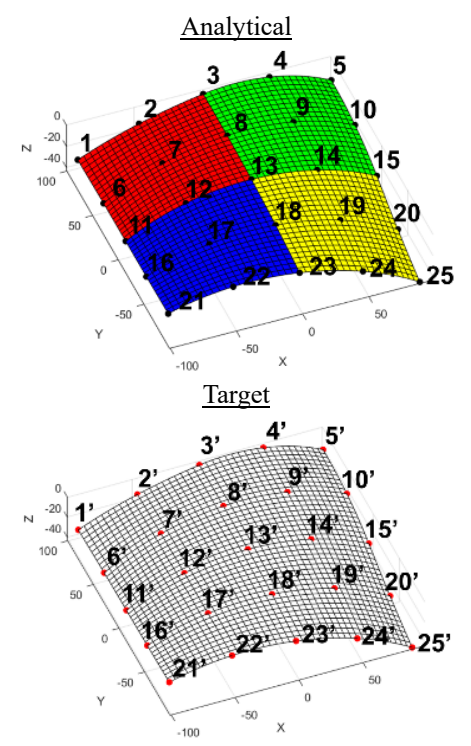


FIGURE 6: FIT-POINTS FOR ANALYTICAL AND TARGET SHAPES

The fitness function could be given as,

$$fitness = \sum_{i=1}^{9} (x_i - x_{i'})^2 + \sum_{i=1}^{9} (y_i - y_{i'})^2 + \sum_{i=1}^{9} (z_i - z_{i'})^2$$
(12)

Where x_i, y_i, z_i are the coordinates of the fit-points of the obtained shape, while $x_{i'}, y_{i'}, z_{i'}$ are those of the target shape. Considering the size of the laminate, the number of fit points used to calculate the fitness function were set as 25 as shown in Figure 6. The 25 fit points are sufficient to capture the shape of the laminate accurately, as each patch is characterized by 9 coordinates at the Face Centered Central Composite (CCF) locations.

The fiber orientations are assigned the following bounds,

$$-90^{\circ} \le \theta_{(p)} \le 90^{\circ}$$
 where p (patch no.) = 1,2,3,4

To ensure manufacturability of the laminates, the following manufacturing constraint for minimum patch size can be enforced. As seen in Figure 5, x', y' are the variables that control

the individual patch sizes. To ensure ease of manufacturing the following bounds are assigned,

$$50mm \le x' \le 150mm$$
$$50mm \le y' \le 150mm$$

Since the size of the four-patch laminate is 200*200mm, these bounds ensure a minimum patch size of 50*50mm and maximum of 150*150mm. Additionally, a step of 5° and 1 mm is set for the fiber orientation and dimensional variables, respectively. This is again done keeping manufacturability in mind.

The higher-level optimization can thus be setup as follows,

minimize fitness

subject to Manufacturing constraints

D.V
$$\theta_1, \theta_2, \theta_3, \theta_4, x', y'$$

Another aspect to consider is the ability of these multi-patch laminates to take up two or more shapes. As discussed in the literature the stable state of a laminate coincides with the minimum strain energy obtained from the lower-level optimization. Thus, a multi-patch laminate would have multiple shapes with minimum strain energy value. In the following sections two approaches are discussed: (i) *Single-state optimization*, which deals with targeting a single state and, (ii) *Two-state optimization*, which deals with targeting two shapes: pre-snapped and post-snapped states.

4.1 Single-state Optimization

As discussed, this optimization setup is used to target a single shape. Figure 7 illustrates the flowchart of the optimization. As seen in the flowchart, the lower level or inner loop constitutes Algmuni's analytical model discussed in detail in the literature review. The inner loop solves for the shape of the laminate based on the parameters passed from the higher-level or the outer loop which are the fiber orientations θ_1 , θ_2 , θ_3 , θ_4 and the dimensions x', y' of the laminate. These parameters are taken as the inputs for this level and the total strain energy (S.E) of the laminate which is the summation of the individual energies of the patches as shown in Eq(11) is expressed in terms of the unknown coefficients of the approximations in Eq(9). The total strain energy is thus minimized to solve for the unknown coefficients. The coefficients can then be substituted into the displacement equations (4) & (5) to obtain the equations of u, vand w as f (x,y). The fit-points can now be calculated from these equations and used to calculate the fitness function in Eq(12) which is to be minimized in the higher-level or the outer loop using a genetic algorithm (GA).

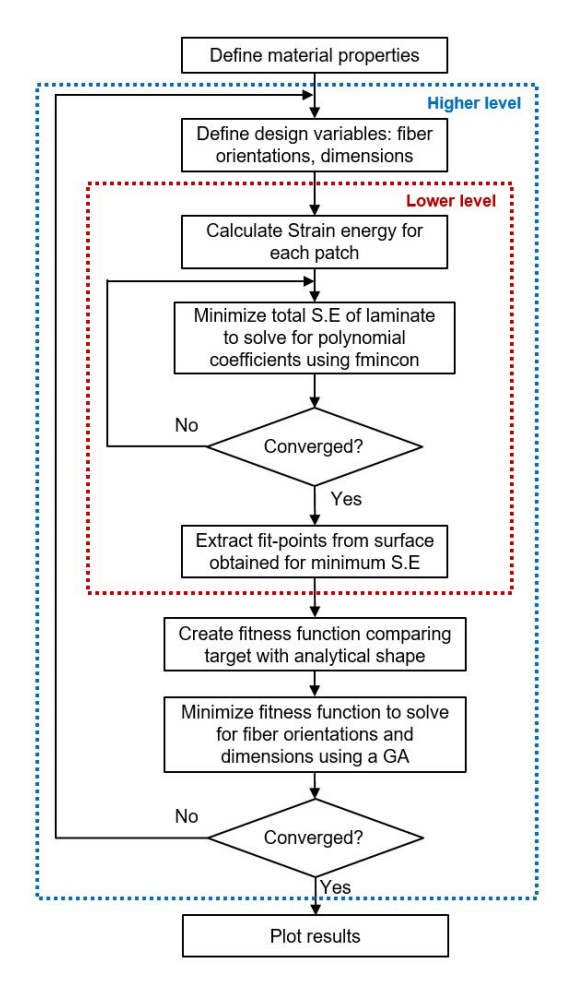


FIGURE 7: OPTIMIZATION FLOWCHART FOR TARGETING SINGLE SHAPE

4.2 Two-state Optimization

In this section the approach to target two shapes: presnapped and post-snapped shape, are discussed. A point to keep in mind is that as discussed earlier an n patch laminate can have a maximum of 2^n stable states. But in this research, we limit the number of shapes to be targeted to two, because solving for more than two states is extremely tedious since the solution is very sensitive to the initial guess. This approach is an extension of the previous approach with the addition of the extra block to calculate the shape of the second stable state. Figure 8 illustrates the flowchart of the optimization setup to target the two shapes.

As discussed in the literature, the stable state of a laminate corresponds to the minimized strain energy for the given configuration. Thus, like the bistable laminate, the four-patch grid laminate will also have multiple minima. The task here is to solve for the multiple minima. To solve for the stable shapes, Algmuni's model has been coded on Matlab and *fmincon* is used to minimize the strain energy equation. The solver can converge to multiple minima using appropriate initial guesses. The next task is to make the choice of the initial guess and this can be done by using the following method as described by the flowchart in Figure 9.

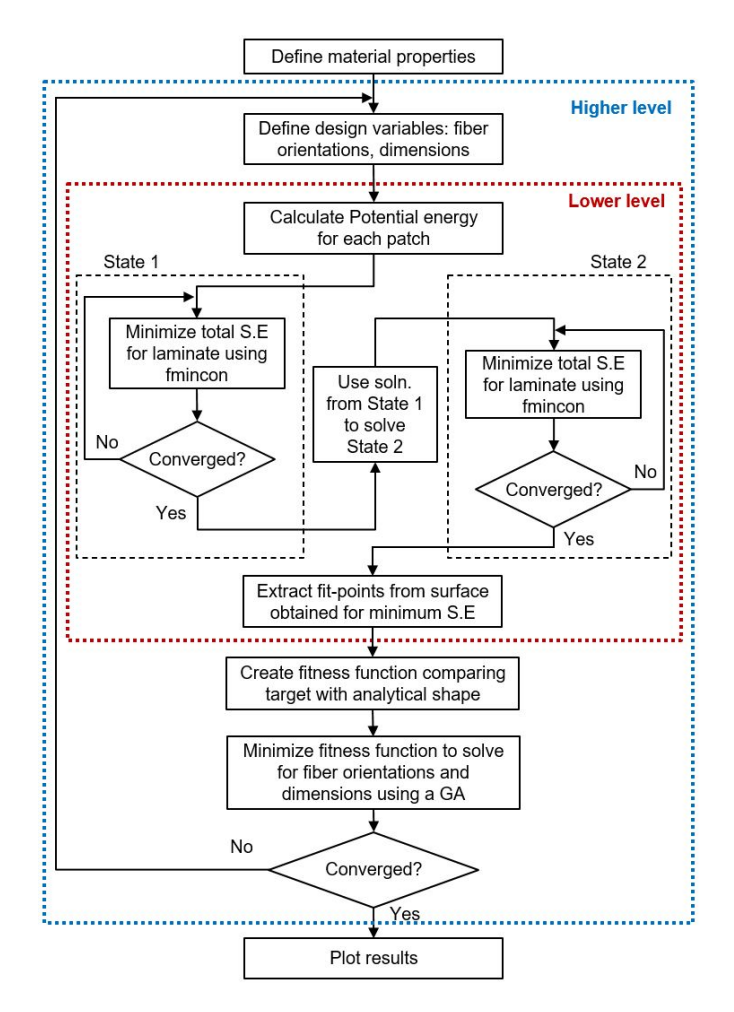


FIGURE 8: OPTIMIZATION FLOWCHART FOR TARGETING TWO SHAPES

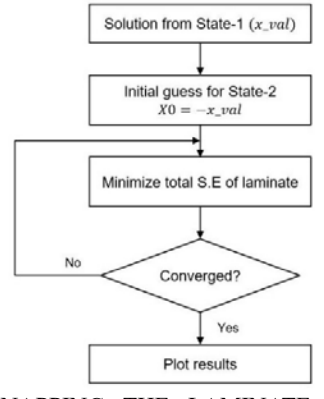


FIGURE 9: SNAPPING THE LAMINATE FROM STATE-1 SOLUTION

As seen in the flowchart in above, the solution for state-1 is multiplied by (-1) and is used as the initial guess for solving for state-2. This is done because the curvatures of the second state

are reversed, thus the values of the coefficients can be negated and set as the initial guess for the second optimization.

Thus, restating the optimization problem for the two-state optimization we have,

Lower level:

The problem formulation largely remains the same. The objective function is the total strain energy of the four-patch grid laminate Π_{total} as shown in Eq(11) and the constraints are the continuity constraints as shown in Table 1. The difference is that in this case, the two states are solved in sequence as shown in the flowchart. Thus, there are two sets of optimizations in the lower level. The solution of the two optimizations which are the unknown coefficients are used to plot the two shapes and the two sets of fit points are calculated to pass to the higher-level optimization.

Higher-level:

The fit points for the two states from the lower level are used to calculate the fitness functions as shown in Eq(12) for each stable state. Thus, the multi- objective optimization problem for this level can be written as,

minimize
$$(fitness 1, fitness 2)$$

subject to Manufacturing constraints
D.V $\theta_1, \theta_2, \theta_3, \theta_4, x', y'$

Thus, *fitness function* 1 corresponds to state-1 and *fitness function* 2 corresponds to state-2. The manufacturing constraints are the same as that explained earlier.

4. RESULTS AND DISCUSSION

In this section, the results for the different iterations of the problem setup are presented and discussed. To solve this optimization the following parameters are kept constant. The laminate has a total size of 200*200mm with four patches and two plies with a ply thickness of 0.15mm. As stated previously the fiber orientation variables are assigned a step size of 5° and the dimensional variables have a step of 1mm. In the inner optimization to minimize strain energy we use *fmincon*, while in the outer optimization we cannot use *fmincon* because we use discrete variables instead of continuous ones, and *fmincon* needs a continuous differentiable function. Thus, a genetic algorithm was considered to solve the problem. Modefrontier was used to setup the problem because it is convenient to create the workflow, assign the step sizes and setup the problem.

For this study we use the laminate as shown in Figure 10, with configuration $\theta = [90^\circ, 30^\circ, 50^\circ, 60^\circ]$ and x' = 80mm, y' = 90mm as the target shape for the optimization. The results for the single and two state optimizations are discussed in the following sections.

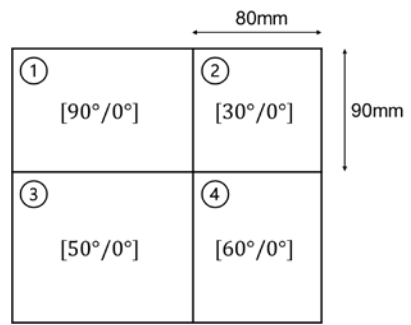


FIGURE 10: TARGET LAMINATE GEOMETRY

4.1 Single-state optimization

For this problem Modefrontier was tied with the Matlab code that ran the analytical model. The inner loop was minimized using *finincon* in Matlab and the outer loop was minimized by the NSGA II algorithm on Modefrontier. The initial population size was set as 50 and the number of generations as 90.

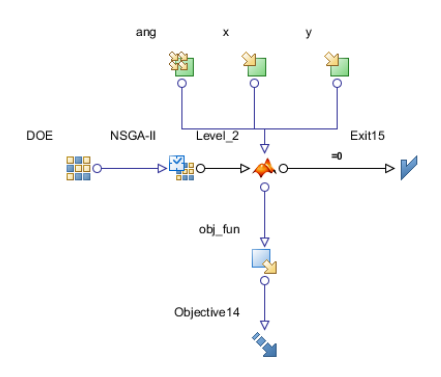


FIGURE 11: OPTIMIZATION WORKFLOW

The workflow for the optimization is shown in Figure 11. In the workflow, the fiber orientations are denoted by 'ang' and the dimensional parameters are denoted by x, y. The objective function to be minimized at the higher level is the fitness function shown in Eq(12). The results for the optimization are as shown in Table 3 below.

TABLE 3: RESULT FOR SINGLE STATE OPTIMIZATION

Target configuration	Optimized configuration
Fiber angles = [90, 30, 50, 60]	Fiber angles = $[70, -50, 60, 40]$
x' = 80mm, y' = 90mm	x' = 95 mm, y' = 94 mm

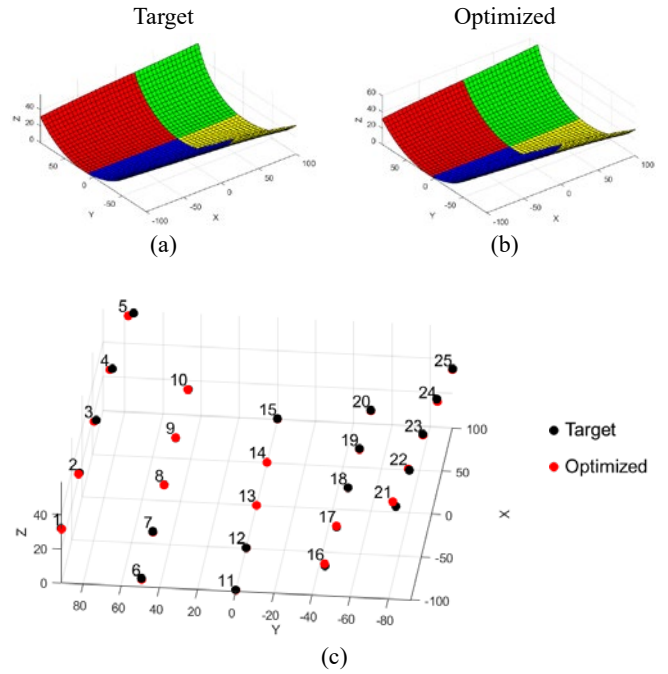


FIGURE 12: OPTIMIZATION RESULTS, (a) TARGET SHAPE, (b) OPTIMIZED SHAPE, (c) COMPARING FIT-POINTS FROM SURFACE IN (a) & (b)

The optimization took 14hrs to run and the minimized fitness function was calculated to be 28.75mm². For a more detailed comparison between the target and the optimized shapes, a simple numerical analysis is presented in Table 4. In the analysis the absolute difference between the z- coordinate values of the fit-points of the two shapes are computed. From the table below we see that the interior points have the least deviations while the corner points 5 and 21 have the largest.

TABLE 4: ABSOLUTE DEVIATION OF Z-COORDINATES

Fit-Point	z coordinate (mm)		Absolute deviation
1 It-1 OIIIt	Target	Optimized	(mm)
1	31.72	31.65	0.07
3	45.88	45.07	0.81
5	59.23	57.64	1.59
11	0.66	0.47	0.19
13	0.00	0.00	0.00
15	0.65	0.47	0.18
21	53.39	55.74	2.35
23	45.88	45.07	0.81
25	34.58	33.90	0.68

As seen from the results of the single-state optimization above, the minimized result captures the target surface well, except for the region around the corner points 5 and 21. Though the values of the design variables do not match the target values, the optimized shape matches the target shape as seen in Figure 12(c). This is because the optimization yields a relatively flat solution domain wherein the interplay between the design

variables of fiber angles and the dimensions results in solutions that are different from the target values yet have a good match with the target shape.

4.2 Two-state optimization

The fitness function from Eq(12) is used to run the two-state optimization and the problem setup and results are discussed ahead. Like the single-state optimization setup, the two-state optimization is also setup on Modefrontier where the inner loop which corresponds to the analytical model is scripted in Matlab and *fmincon* is used to minimize the strain energy, while the outer loop is minimized using the MOGA II algorithm in Modefrontier which is a multi-objective genetic algorithm. The workflow for the optimization is as shown in Figure 13, where 'obj_fun_1' and 'obj_fun_2' are the fitness functions for the two states shapes, respectively.

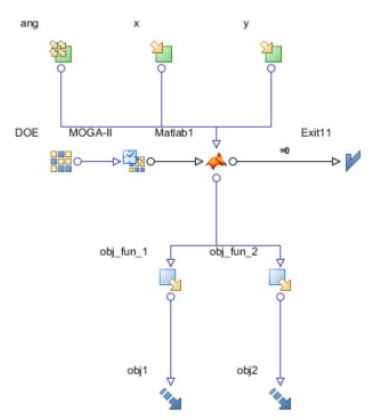


FIGURE 13: TWO-STATE OPTIMIZATION WORKFLOW

The population size was kept as 50 and the GA was run for 90 generations. The optimizer took 47.5hrs to complete the job and the optimized results are as shown Table 5 below.

TABLE 5: RESULT FOR TWO STATE OPTIMIZATION

Target configuration	Optimized configuration	
Fiber angles = $[90, 30, 50, 60]$	Fiber angles = $[90, 30, 50, 60]$	
x' = 80mm, y' = 90mm	x' = 79mm, $y' = 91$ mm	

Figures 14 and 15 illustrate the optimized results for the optimization

State-1

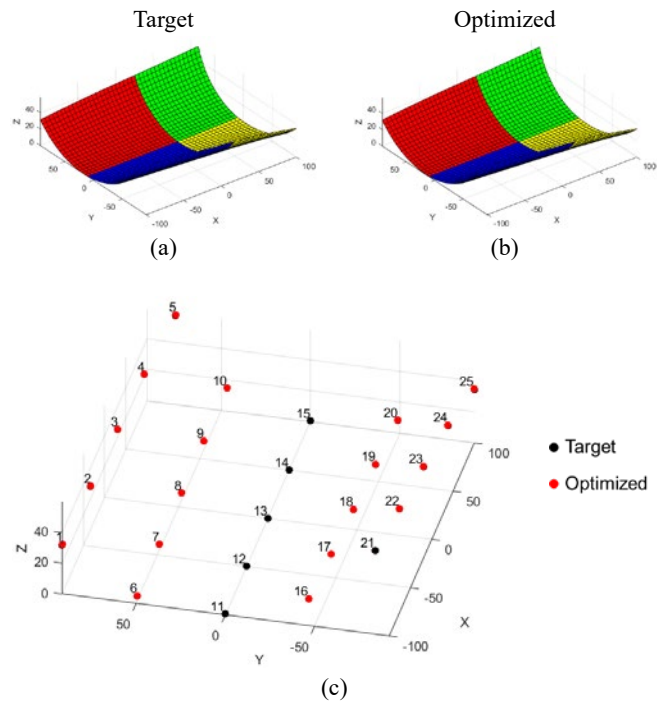


FIGURE 14: STATE-1 OPTIMIZATION RESULTS, (a) TARGET SHAPE, (b) OPTIMIZED SHAPE, (c) COMPARING FIT-POINTS FROM SURFACE IN (a) & (b) *State-2*

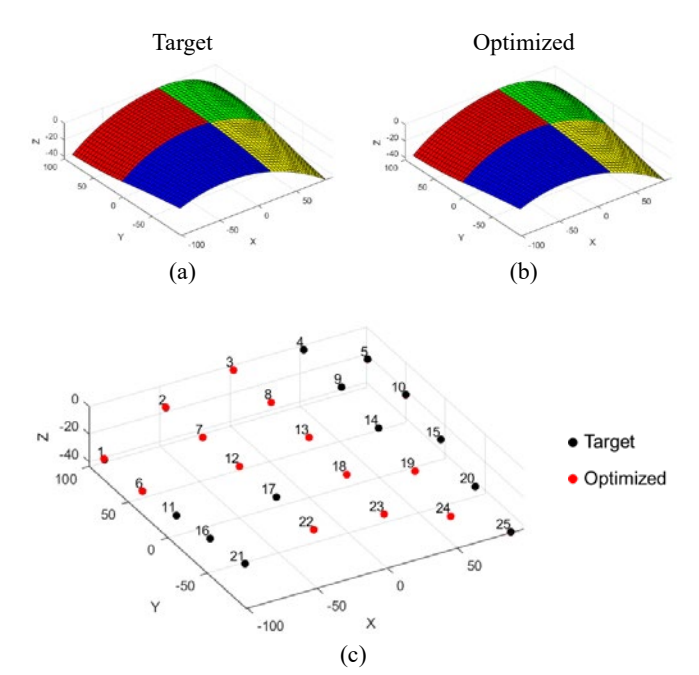


FIGURE 15: STATE-2 OPTIMIZATION RESULTS, (a) TARGET SHAPE, (b) OPTIMIZED SHAPE, (c) COMPARING FIT-POINTS FROM SURFACE IN (a) & (b)

From these results we can observe that the GA is able to reach a solution that is very close to the target values with fitness function values close to zero, which is the target. This result is more accurate than the single-state result because the second objective function pushes the GA to search for better designs where the fitness functions for both states are minimized. This can be seen in Figure 16 where the designs for the two-state optimization are plotted on a scatter chart of fitness 1 vs fitness 2. The optimum design that matches the target laminate parameters should converge at (0,0), which it does in the twostate optimization implying that both target shapes are achieved. But from the plot we see multiple designs close to the x and y axes, which explains the presence of multiple minima when targeting single shapes. This explains the discrepancy in the fiber orientation and dimensions of the single-state optimized result in spite of the good fit between target and optimized shapes.

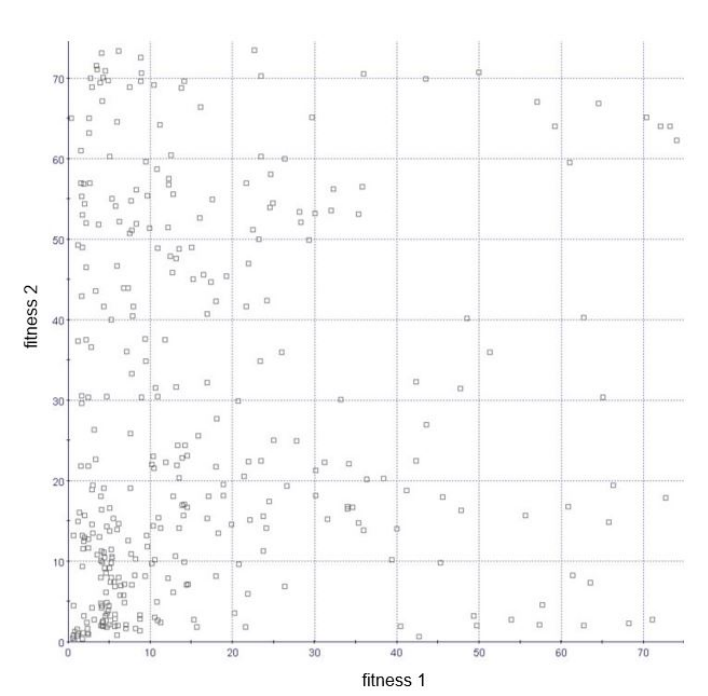


FIGURE 16: SCATTER CHART OF FITNESS 1 VS FITNESS 2

5. CONCLUSION

This paper aims at establishing a method to design multipatch laminates by utilizing the mechanics models present in the literature. For this study, a four-patch 2-ply laminate was considered, and the top fiber orientations and the patch dimensions were parameterized, and a bi-level optimization was set up which minimized the strain energy and the fitness function of the laminate in the lower and higher levels, respectively. The optimization was run for targeting single and two states and the resulting solution matches the target shape. The results of the optimization indicate that this approach to designing multi-patch laminates has some merit and is currently being extended to a greater number of patches.

ACKNOWLEDGEMENTS

This study is supported by the National Science Foundation NSF grant 1760943: "Establishing a Design Framework for Multi-functional composites by Leveraging Kirigami Cutting, Multi-stability, and Multi-level Optimization." Any opinions, findings, and conclusions or recommendations expressed in this material are those of the author(s) and do not necessarily reflect the views of the National Science Foundation.

REFERENCES

- [1] Dano, M., and Hyer, M. W., "Thermally-Induced Deformation Behavior of Unsymmetric Laminates," Int. J. Solids Struct., 35(17) (1998): pp. 2101–2120.
- [2] Schlecht, M., and Schulte, K., "Advanced Calculation of the Room-Temperature Shapes of Unsymmetric Laminates," J. Compos. Mater., 33(16) (1999): pp. 1472–1490.
- [3] Dano, M. L., and Hyer, M. W., "Snap-through of Unsymmetric Fiber-Reinforced Composite Laminates," Int. J. Solids Struct., 40(22) (2000): pp. 5949–5972.
- [4] Diaconu, C. G., Weaver, P. M., and Mattioni, F., "Concepts for Morphing Airfoil Sections Using Bi-Stable Laminated Composite Structures," Thin-Walled Struct., 46(6) (2008): pp. 689–701.
- [5] Panesar, A. S., and Weaver, P. M., "Optimisation of Blended Bistable Laminates for a Morphing Flap," Compos. Struct., 94(10) (2012): pp. 3092–3105.
- [6] Betts, D. N., Salo, A. I. T., Bowen, C. R., and Kim, H. A., "Characterisation and Modelling of the Cured Shapes of Arbitrary Layup Bistable Composite Laminates," Compos. Struct. (2010)
- [7] Algmuni, A., Xi, F., and Alighanbari, H., "Design and Analysis of a Grid Patch Multi-Stable Composite," Compos. Struct., 246 (2020): p. 112378.
- [8] Mattioni, F., Weaver, P. M., and Friswell, M. I., "Multistable Composite Plates with Piecewise Variation of Layup in the Planform," Int. J. Solids Struct., 46(1) (2009): pp. 151–164.
- [9] Jones, R. M., "Mechanics of Composites Materials," (1999).